Molecular Vision 2018; 24:603-612 <http://www.molvis.org/molvis/v24/603>
Received 24 April 2018 | Accepted 29 August 2018 | Published 31 August 2018

Novel homozygous splicing mutations in *ARL2BP* cause autosomal recessive retinitis pigmentosa

Alessia Fiorentino,[1] Jing Yu,[2] Gavin Arno,[1,3] Nikolas Pontikos,[1] Stephanie Halford,[2] Suzanne Broadgate,[2] Michel Michaelides,[1,3] Keren J. Carss,[4,5] F. Lucy Raymond,[5,6] Michael E. Cheetham,[1] Andrew R. Webster,[1,3] Susan M. Downes,[7] Alison J. Hardcastle,[1] for the NIHR-BioResource Rare Diseases Consortium, the U.K. Inherited Retinal Dystrophy Consortium

(The last three authors (Drs. Webster, Downes, and Hardcastle) are co-senior authors for this study.)

[1]UCL Institute of Ophthalmology, London, UK; [2]Nuffield Laboratory of Ophthalmology, Nuffield Department of Clinical Neurosciences, University of Oxford, John Radcliffe Hospital, Oxford, UK; [3]Moorfields Eye Hospital, London, UK; [4]Department of Haematology, University of Cambridge, NHS Blood and Transplant Centre, Cambridge, UK; [5]NIHR BioResource - Rare Diseases, Cambridge University Hospitals NHS Foundation Trust, Cambridge Biomedical Campus, Cambridge, UK; [6]Department of Medical Genetics, Cambridge Institute for Medical Research, University of Cambridge, Cambridge, UK; [7]Oxford Eye Hospital, John Radcliffe Hospital, Oxford, UK

Purpose: Mutations in *ARL2BP,* encoding ADP-ribosylation factor-like 2 binding protein, have recently been implicated as a cause of autosomal recessive retinitis pigmentosa (arRP), with three homozygous variants identified to date. In this study, we performed next-generation sequencing to reveal additional arRP cases associated with *ARL2BP* variants.
Methods: Whole-genome sequencing (WGS) or whole-exome sequencing (WES) was performed in 1,051 unrelated individuals recruited for the UK Inherited Retinal Disease Consortium and NIHR-BioResource Rare Diseases research studies. Sanger sequencing was used to validate the next-generation sequencing data, and reverse transcriptase (RT)–PCR analysis was performed on RNA extracted from blood from affected individuals to test for altered splicing of *ARL2BP*. Detailed phenotyping was performed, including clinical evaluation, electroretinography, fundus photography, fundus autofluorescence imaging, and spectral-domain optical coherence tomography.
Results: Homozygous variants in *ARL2BP* (NM_012106.3) were identified in two unrelated individuals with RP. The variants, c.207+1G>A and c.390+5G>A, at conserved splice donor sites for intron 3 and intron 5, respectively, were predicted to alter the pre-mRNA splicing of *ARL2BP*. RT–PCR spanning the affected introns revealed that both variants caused abnormal splicing of *ARL2BP* in samples from affected individuals.
Conclusions: This study identified two homozygous variants in *ARL2BP* as a rare cause of arRP. Further studies are required to define the underlying disease mechanism causing retinal degeneration as a result of mutations in *ARL2BP* and any phenotype-genotype correlation associated with residual levels of the wild-type transcript.

Retinitis pigmentosa (RP; OMIM: 268000) is the most common inherited retinal dystrophy, affecting approximately 1 in 3,000 individuals [1]. RP is characterized by progressive degeneration of the retina, typically starting in the midperiphery and advancing toward the macula and fovea. Affected individuals commonly present with nyctalopia and peripheral visual field constriction, with significant loss of central vision as the macular cones become involved at later stages of disease progression [2]. RP can occur in isolation (non-syndromic RP) or with additional systemic manifestations (syndromic RP). The genetic etiology of RP is remarkably heterogeneous, with autosomal-dominant, autosomal-recessive, and X-linked modes of inheritance and at least 86 disease-causing genes identified for the autosomal-recessive form alone (The Retinal Information Network; accessed February 7, 2018). The genes implicated are involved in numerous pathways in the retina, including phototransduction, retinal metabolism, RNA splicing, and ciliogenesis [3,4].

Variants in genes coding for proteins involved in the cilia structure or function account for at least 36% of genetically diagnosed cases of RP, and can be classified as ciliopathies based on protein localization and function [5]. Mutations in ciliopathy genes can cause isolated RP or syndromic disease, such as Bardet-Biedl syndrome and Usher syndrome [5-7]. Cilia assembly and maintenance require coordinated intraflagellar transport of proteins from the basal body along the axoneme to the tip of the cilium, fundamental not only for phototransduction but also for photoreceptor survival [8,9]. *ARL2BP* (Gene ID: ENSG00000102931, OMIM: 615407) encodes ADP-ribosylation factor-like 2 (ARL2) binding

Correspondence to: Alison J. Hardcastle, UCL Institute of Ophthalmology, 11-43 Bath Street, EC1V 9EL, London, United Kingdom; Phone: +44(0)2076086945; FAX: +44(0)2076086892; email: a.hardcastle@ucl.ac.uk

protein (ARL2BP or BART). It is an effector protein of the small GTP-binding proteins ARL2 and ARL3, and localizes to the distal part of the connecting cilium in photoreceptors and to the basal body of ciliated cells [10]. Three variants in *ARL2BP* in three unrelated families have been previously reported as causative of RP, with or without situs inversus [10,11].

The identification of disease-causing mutations in RP has been accelerated by the implementation of next-generation sequencing (NGS) technologies. For affected individuals who lack a molecular diagnosis, whole-exome sequencing (WES) and whole-genome sequencing (WGS) are effective tools for identifying new potential causative variants [12].

In our collaborative study of unsolved cases, through the UK Inherited Retinal Disease Consortium and NIHR-BioResource Rare Diseases research study, 1,051 unrelated individuals were analyzed with WES or WGS. In this report, we describe two unrelated families, with no known consanguinity, in whom WES or WGS revealed homozygous variants affecting the mRNA processing of *ARL2BP*.

METHODS

Clinical assessment of study families: The study protocols adhered to the tenets of the Declaration of Helsinki and received approval from the local Ethics Committee of the participating institutions: Moorfields Eye Hospital and Oxford Eye Hospital. Written, informed consent was obtained from all participants before they were included in this study. The two probands underwent detailed clinical examination, including best-corrected decimal visual acuity (BCVA), 35-degree color fundus photography (TRC-NW8; Topcon (Great Britain) Medical Ltd., Newbury, UK), ultrawidefield confocal scanning laser imaging (Optos plc, Dunfermline, UK), fundus autofluorescence (FAF) imaging (Spectralis, Heidelberg Engineering Inc., Carlsbad, CA), and spectral-domain optical coherence tomography (SD-OCT; Spectralis, Heidelberg Engineering Inc.).

Next-generation sequencing: DNA samples for the two probands were analyzed with WES in family 1 [13] and WGS in family 2 [12] as follows. For the WES analysis, genomic DNA was processed according to the Agilent SureSelect XT Library Prep protocol (Agilent Technologies, Santa Clara, CA) with capture using a SureSelect Exome V5 Capture library. After hybridization and indexing, 100 bp paired end sequencing was performed (Illumina HiSeq 2500 sequencer, Illumina Inc., San Diego, CA). Reads were aligned to the hg19 human reference sequence (build GRCh37) using Novoalign v.2.08 (Novocraft, Selangor, Malaysia). Duplicate reads were marked with Picard tools MarkDuplicates. Variant calling was performed using GATK, creating gVCF formatted files for each sample. The final variant calling for individual gVCF files was performed using the GATK Genotype gVCFs module. The variant quality scores were then recalibrated separately for indels and single nucleotide variants (SNVs). Resulting variants were annotated using ANNOVAR based on Ensembl gene and transcript definitions. Candidate variants were filtered based on function (non-synonymous, presumed loss-of-function, or splicing) and a minor allele frequency (MAF) of <0.005 using several data sets, including an in-house exome-sequencing control data set of approximately 4,000 individuals (UCLEx), NHLBI GO Exome Sequencing Project (EVS), and 1000 Genomes phase 1 data set. Variants were further manually interrogated for variant call quality, predicted pathogenicity, and biologic plausibility. Candidate variants were then ranked, considering the likely mode of inheritance for each family, prioritizing variants with a MAF of <0.001 in the Exome Aggregation Consortium (ExAC) database [14] (accessed on 11/01/2017).

WGS was performed using an Illumina TruSeq DNA PCR-Free Sample preparation kit (Illumina, Inc.) and an Illumina HiSeq 2500, generating minimum coverage of 15X for approximately 95% of the genome. Reads were aligned to GRCh37 using Isaac Genome Alignment Software (version 01.14; Illumina, Inc.) [15]. SNVs and small insertion/deletions were identified using Isaac Variant Caller (version 2.0.17). To identify potentially pathogenic variants, a two-step variant filtering protocol was designed, using automated filtering followed by a manual review. For SNVs and indels, automated filtering identified variants that fulfill the following criteria: passes standard Illumina quality filters in >80% of the whole NIHR BioResource Rare Diseases cohort (n=6,688); predicted to be a high impact, medium impact, or splice region variant, or present in the HGMD Pro database; and had a MAF <0.01 in the control data sets, including the NIHR BioResource Rare Diseases cohort and the Exome Aggregation Consortium (ExAC) database [14]. If a variant was present in the HGMD Pro database, a higher MAF threshold of 0.1 was used. A manual review of all the variants that passed the automated filtering was then performed.

For WES and WGS, candidate variants were then prioritized based on previous association of the gene with a compatible phenotype and biologic plausibility. Phenopolis [16], a platform for studying the pleiotropy of genes, was also used to prioritize variants. Copy number variations (CNVs) in the genomic region spanning the *ARL2BP* gene were assessed in the WES data using the Exome Depth calling algorithm [17] and WGS data using Isaac Copy Number Variant Caller

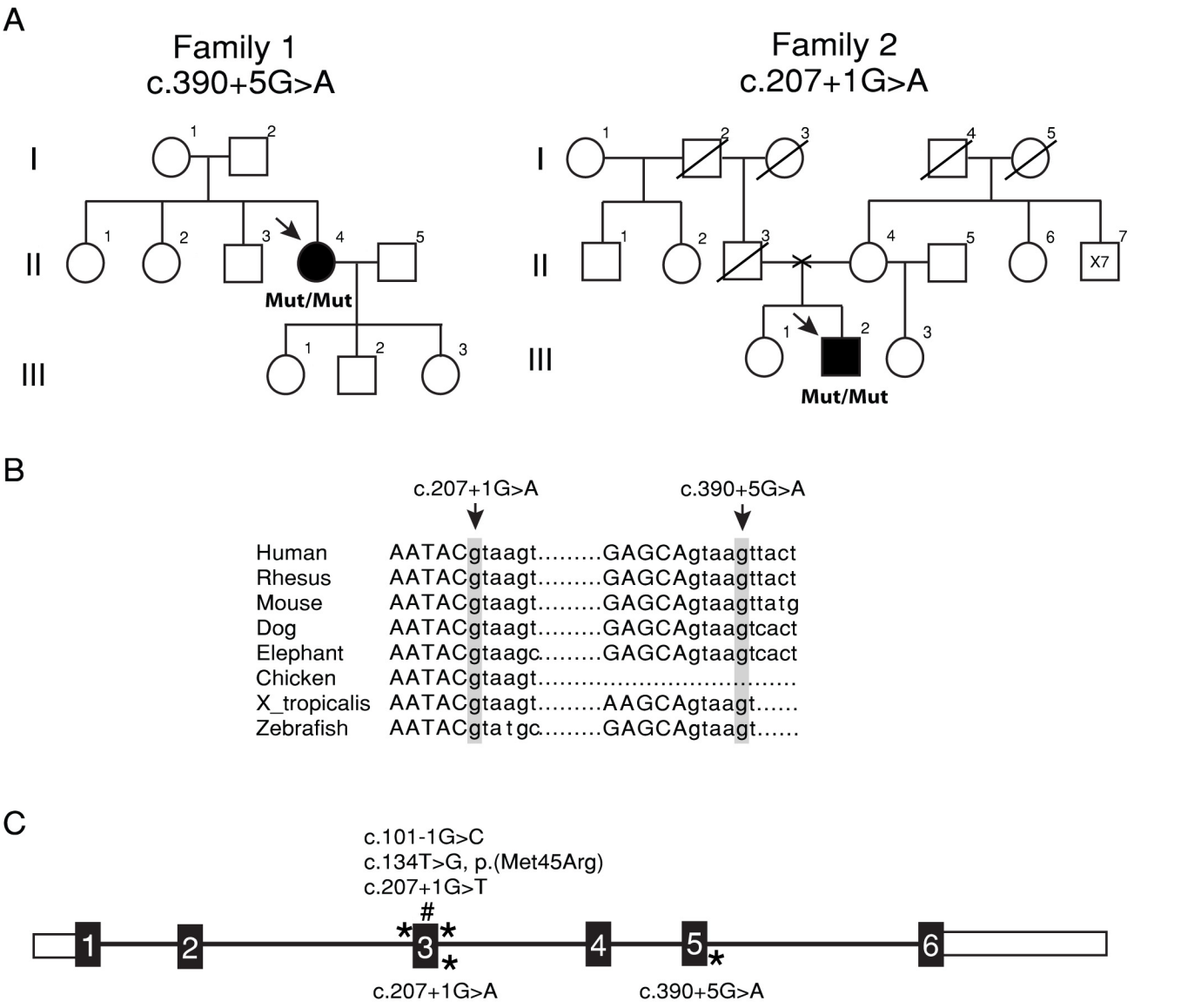

Figure 1. Homozygous *ARL2BP* mutations in families with autosomal recessive retinitis pigmentosa. **A**: Pedigrees of two study families. The arrow indicates the affected proband in each family. The mutation in *ARL2BP* (NM_012106.3) identified in each family is indicated. Mut=*ARL2BP* mutation present. **B**: Multiple DNA sequence alignment of orthologs shows that the donor splice site sequences and site of mutations (c.207+1 and c.390+5) are highly conserved across different species. **C**: Schematic of the genomic structure of *ARL2BP*. Positions of mutations in *ARL2BP* identified in this study (below the gene structure) and previously identified mutations (above the gene structure) are indicated (not to scale).

(Canvas, Illumina) and Isaac Structural Variant Caller (Manta, Illumina) [12].

Sanger sequencing: PCR amplification and bidirectional Sanger sequencing were performed using Go taq Green Master Mix (Promega, Madison, WI) with primers flanking the variants (Family 1 c.390+5G>A: forward primer CAT CTG TTC CG TTT GCA GGC, reverse primer GCC AGT TTG AAG GGA GAA TGA TG; Family 2 c.207+1G>A: forward primer CCA CAT CAG GGT CCC ATT TA, reverse primer CCA CCT CAA CCT CCC AAA TA). 50 ng of DNA and a final concentration of 0.4 µM of each mutation-specific forward and reverse primer were used for amplification in a final volume of 12.5 µl. Amplification was performed for 35 cycles, each cycle consisted of 30 s at 95 °C, 30 s at 62 °C, and 30 s at 72 °C.

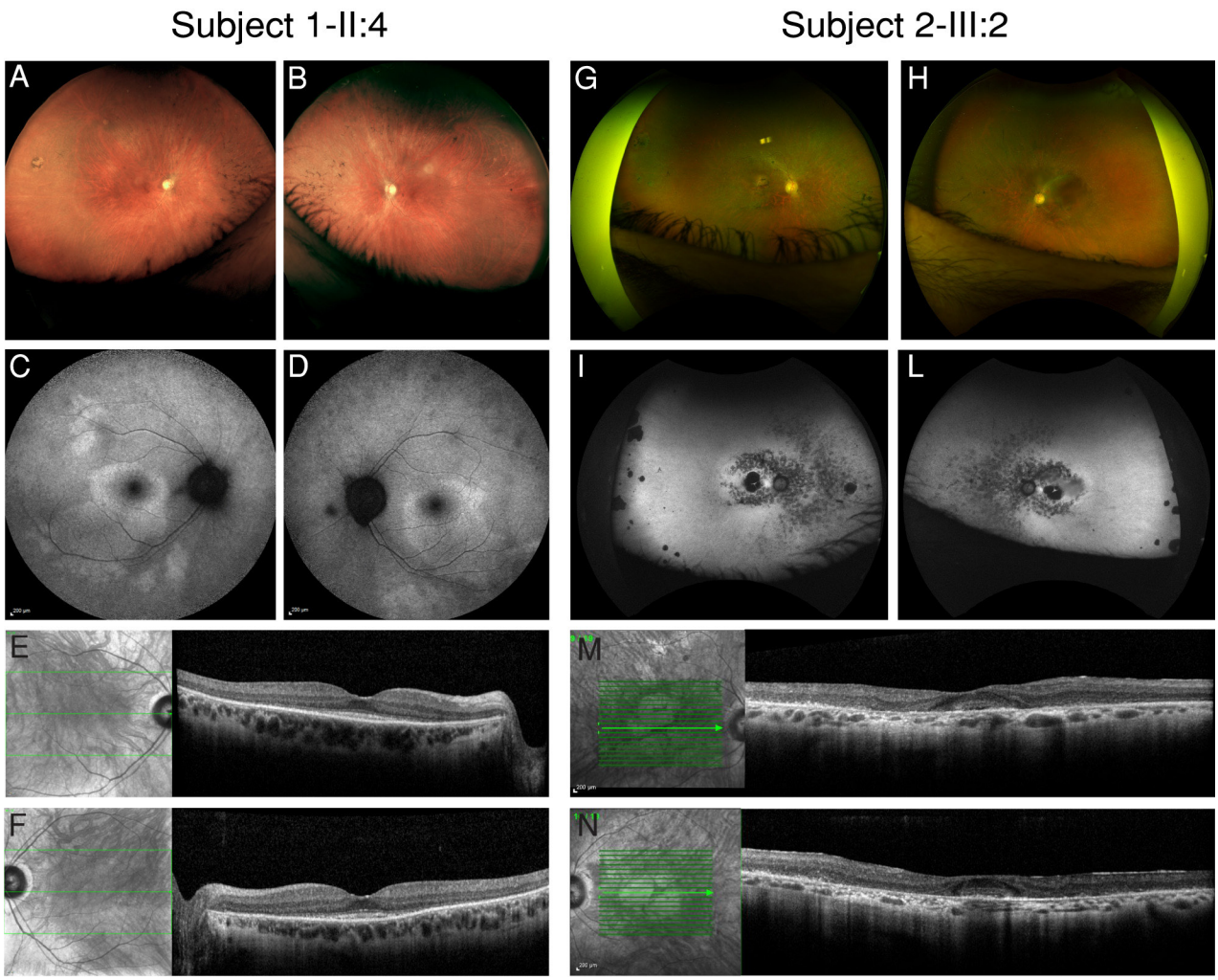

Figure 2. Retinal imaging of the probands of family 1 and family 2. Family 1. **A**, **B**: Optos widefield color fundus imaging showing intraretinal bone spicule-like pigmentation mainly in the nasal retina, generalized vascular attenuation, and optic nerve pallor. **C**, **D**: Autofluorescence imaging (Heidelberg Spectralis) showing inferiorly a reduced signal intensity in the outer macula and the midperiphery compatible with the loss of the outer retinal structure in these areas. Conversely, the foveal region appears intact bilaterally. **E, F**: Spectralis optical coherence tomography (OCT) images of the proband showing normal macular architecture. Family 2. **G**, **H**: Optos widefield color fundus imaging showing bilateral macular atrophy, and outer retinal atrophy along the vascular arcades, with scanty bone spicule-like pigmentation mainly in the nasal retina. **I**, **L**: Optos widefield autofluorescence showing reduced signal at the posterior pole, around the arcades, and nasally, with residual autofluorescence at the fovea in both eyes. **M**, **N**: Heidelberg Spectralis infrared and OCT images of the proband, age mid-40s, showing widespread loss of the photoreceptor layers in both eyes, with a degree of preservation of the outer retinal structure at the fovea bilaterally. All images are consistent with widespread loss of the outer retinal structure throughout the fundus bilaterally.

In silico analysis of ARL2BP variants: The UCSC genome browser and Phenopolis [16] were used for visualization of existing gene variants and evolutionary conservation. Variants in *ARL2BP* were scored for likelihood of altering splicing using several tools: Berkeley Drosophila Genome Project Splice Site Prediction [18], NetGene2 [19], and Human Splice Finder.

Reverse transcriptase–PCR analysis of ARL2BP: Total RNA was extracted from whole blood using blood PAXgene Blood RNA collection tubes and a PAXgene Blood purification RNA Kit (PreAnalytix, Qiagen/BD, Hombrechtikon, Switzerland). cDNA was reverse-transcribed using a cDNA synthesis kit with an Oligo (dT) Primer mix (Tetro cDNA Syntesis kit, Bioline, Toronto, Canada). The cDNA was then amplified from exon 1 (forward primer 5′-CTT TCT CCT CCG CCT CTG AT-3′) to exon 6 (reverse primer 5′-TCA

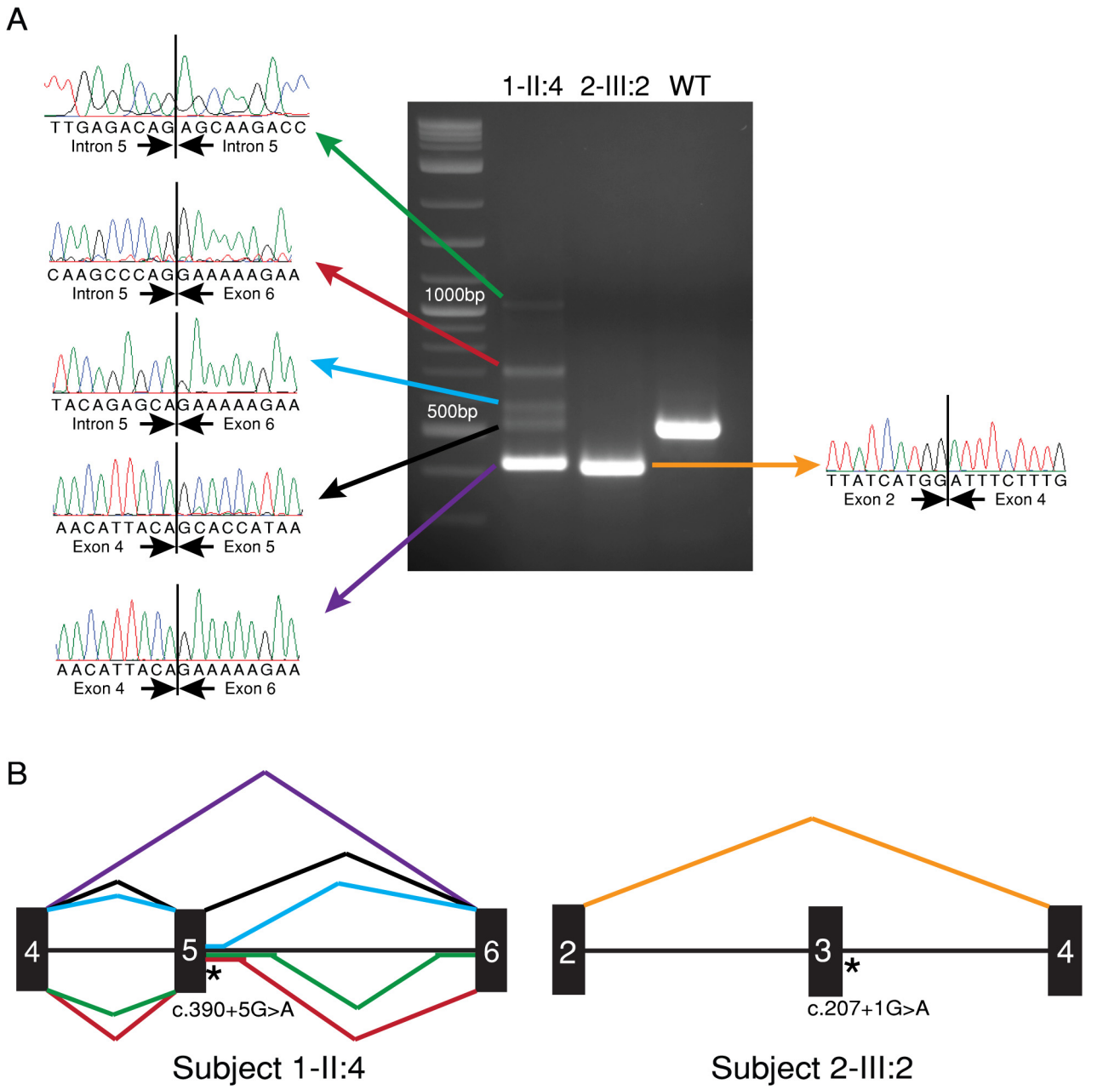

Figure 3. Aberrant pre-mRNA splicing of *ARL2BP* as a consequence of homozygous donor splice site mutations. **A**: Agarose gel electrophoresis showing the reverse transcriptase (RT)–PCR products (exon 1 to exon 6) from whole blood RNA for affected individuals from family 1 (1-II:4), family 2 (2-III:2), and a control individual (wild type, WT), as indicated. Multiple *ARL2BP* transcripts were amplified (forward primer 5′-CTT TCT CCT CCG CCT CTG AT-3′, reverse primer 5′-TCA TGA GCT GAG CCT ATT GG-3′) for individual 1-II:4, who is homozygous for the c.390+5G>A exon 5 donor site variant. RT–PCR products range in size from 429 bp to 1,035 bp due to aberrant splicing of *ARL2BP*. Corresponding electropherograms are shown for each transcript. A low level (7.1%) of the WT transcript was also detected. An abnormal 419 bp transcript was amplified using the same primers in individual 2-III:2, who is homozygous for the c.207+1G>A exon 3 donor splice site variant. The product was due to exon 3 skipping, shown in the corresponding electropherogram. **B**: Schematic representation of the aberrant splicing events identified in individuals homozygous for the c.390+5G>A and c.207+1G>A variants in *ARL2BP*. Each splicing variant is color coded according to the arrows shown in panel A, corresponding to the transcripts detected with RT–PCR. Exons are represented by rectangles and introns by lines. * represents the location of the variant.

TGA GCT GAG CCT ATT GG-3′) to amplify the *ARL2BP* transcripts. 1 µl of cDNA and a final concentration of 0.4 µM of each primer were used for amplification in a final volume of 25 µl using Go taq Green Master Mix (Promega). Amplification was performed for 35 cycles, each cycle consisted of 30 s at 95 °C, 30 s at 62 °C, and 30 s at 72 °C. The resulting products were then gel purified (QIAquick Gel Extraction Kit, Qiagen, Hilden, Germany) and Sanger sequenced to determine the transcripts produced by alternative splicing. Quantification of different transcripts was calculated using Image Lab Software 6.0.1 (Bio-Rad, Hercules, CA).

RESULTS

ARL2BP variants identified in individuals with retinitis pigmentosa: Using a combination of WES and WGS, variants in *ARL2BP* were identified in two unrelated individuals with RP. The pedigrees of the study families are shown in Figure 1A.

A simplex white female (1-II:4) from a non-consanguineous family (family 1) was diagnosed with RP aged 35 years. No other syndromic features were identified. WES was performed, and variants were filtered and prioritized as described, considering potential recessive inheritance. This identified a homozygous *ARL2BP* variant, c.390+5G>A, as the most compelling candidate (GRCh37 Chr16:57284424G>A, NM_012106.3: c.390+5G>A). This variant was absent in the gnomAD database [14] and was predicted by NetGene2, NNsplice, and Human Splice Finder to disrupt the donor splice site of exon 5. No CNVs were detected in *ARL2BP*. Sanger sequencing confirmed the variant in the affected female proband.

The proband (GC21134, 2-III:2) of family 2, from a North African non-consanguineous family (self-reported), was diagnosed with RP at age 36 years. WGS was performed as part of the NIHR-BioResource Rare Diseases research study [12], and variants were filtered and prioritized as described considering potential recessive inheritance. A homozygous variant, c.207+1G>A, in *ARL2BP* (GRCh37 Chr16:57282556G>A, NM_012106.3: c.207+1G>A) was identified as the most probable cause of disease. The variant alters the invariant GT dinucleotide at the splice donor site of exon 3. This variant has an MAF of 0.0001071 in the gnomAD database [14], consistent with an allele frequency for a recessive condition, with no homozygous individuals present in the database. The variant was predicted by NetGene2, NNsplice, and Human Splice Finder to disrupt the donor splice site of exon 3. Sanger sequencing confirmed the variant in the affected male proband. No CNVs were detected in *ARL2BP*. Both variants are located at highly conserved splice donor sites in *ARL2BP* (Figure 1B).

Phenotypic comparison of affected individuals: A white female (1-II:4) presented at 35 years of age with slow dark adaptation and mild photosensitivity. There was no family history of inherited eye disease, and general health was excellent, with no syndromic features. After 7 years of follow-up, at age 42 years, she had normal visual acuity of OD 0.04 LogMAR (6/6 Snellen equivalent) and OS 0.02 (6/6). Goldmann visual field testing at presentation showed generalized constriction to all test targets; although she was able to continue driving until 40 years of age, by which time there was moderate infero- and superotemporal constriction in the left eye and inferotemporal loss in the right eye. Fundoscopy and retinal imaging showed intraretinal bone spicule-like pigmentation mainly in the nasal retina, generalized vascular attenuation, and optic nerve pallor (Figure 2A,B). SD-OCT showed normal macular architecture (Figure 2E,F), but FAF imaging revealed symmetric bilateral perimacular rings of increased signal, also extending bilaterally inferiorly and in the right eye also superiorly, with patchy reduced AF in the midperiphery (Figure 2C,D). Electrophysiological assessment showed greater generalized rod than cone loss, with significant reduction in rod amplitudes (Appendix 1). Other investigations included normal karyotyping and normal phytanic acid levels. There were no signs of situs inversus (self-reported).

A male (2-III:2, GC21134) from a North African non-consanguineous family presented at 36 years of age with night blindness when he was diagnosed with retinitis pigmentosa. There was no family history and no evidence of systemic illness (situs inversus not investigated). Since diagnosis, there has been slow progressive loss of peripheral vision and more recently, of central vision. His BCVAs at age 41 years were 20/60 right and 20/40 left. By 48 years of age, his acuities had decreased to 20/110 (LogMar 0.74) right and 20/83 left (LogMar 0.62). From the age of 41 years, all peripheral visual field outside the central 10 degrees had been lost bilaterally. Images in Figure 2C–H show the extensive degeneration at age 45 years (right more than left).

Fundus examination showed bilateral macular and peripheral retinal atrophy with widespread intraretinal bone spicule-like pigmentation (Figure 2G, H). Fundus autofluorescence (Optos) showed signal reduction at the posterior pole, around the temporal vascular arcades, and throughout the nasal retina (Figure 2I, L). On OCT, there was widespread loss of the outer retinal structure with some preservation of the foveal photoreceptor layer (Figure 2M, N), corresponding to residual autofluorescence at the fovea (Figure 2I, L).

Table 1. Homozygous variants in *ARL2BP* and their associated phenotype.

Family/Patient	Variant	Situs inversus	Age of diagnoses	Visual acuity (Logmar, Snellen)		Macula involvement	Partial WT expression
				RE	LE		
GC19277/IV-3 [10]	c.134T>G, p. Met45Arg	absent	20s	0.25 (20/36)	0.5 (20/63)	present	NR
MOL0807/IV-1 [10]	c.101–1G>C	present	20s	HM	PL	present	NR
MOL0807/IV-2 [10]	c.101–1G>C	present	20s	0.2 (20/32)	0.4 (20/40)	present	NR
MOL0807/IV-3 [10]	c.101–1G>C	absent	20s	NR	NR	present	present
CIC01154 [11]	c.207+1G>T	absent	teens	1 (20/200)	CF	present	absent
CIC01155 [11]	c.207+1G>T	absent	teens	0.097 (20/25)	0.097 (20/25)	present	NR
1/1-II:4	c.390+5G>A	NR	35	0.04 (20/20)	0.02 (20/20)	absent	present
2/2-III:2 (GC21134)	c.207+1G>A	NI	36	0.74 (20/110)	0.62 (20/83)	present	absent

CF=counting fingers, HM=hand motion, PL=light perception, NI=not investigated, NR=not reported. [10], and [11] refer to previous reports in the references.

ARL2BP variants alter pre-mRNA splicing: RT–PCR analysis was performed on cDNA derived from RNA extracted from blood samples for the two affected individuals and controls, and the resulting transcripts were Sanger sequenced. *ARL2BP* transcripts in affected individuals were aberrantly spliced (Figure 3).

In individual 1-II:4, the homozygous c.390+5G>A mutation within the donor splice site for exon 5 resulted in five different transcripts: Four transcripts revealed abnormal splicing events, including exon 5 skipping and intron 5 inclusion, predicted to result in premature termination of the protein (Figure 3A). Exon 5 was skipped in the most abundant transcript (representing 75.2% of the total transcript), resulting in a frameshift and premature termination p.(His99Lysfs*9; NM_012106.3). In three other aberrant transcripts, alternative acceptor and donor sites were activated, resulting in the inclusion of part of intron 5 (Figure 3A, B). The predicted consequence of these events is an insertion of 55 bp, 189 bp, and 509 bp resulting in p.(Glu131Glyfs*9), p.(Glu131_His163delinsGlyLysLeuLeuLeuLeuPheIle), and p.(Glu131Glyfs*9), respectively. These three aberrant transcripts represent 7.2%, 9.1%, and 1.4% of the total transcript, respectively. A normally spliced *ARL2BP* transcript was also detected (Figure 3A) representing only 7.1% of the total transcript. In individual 2-III:2, only one transcript was detected that represents exon 3 skipping, predicted to lead to a frameshift and premature termination codon p.(Asp35Phefs*8; Figure 3A, B).

DISCUSSION

Davidson and colleagues [10] first described biallelic mutations in *ARL2BP* associated with arRP in two families. An additional family was subsequently identified by Audo et al. [11]. These studies described homozygous *ARL2BP* missense and splice site variants (c.101–1G>C, c.134T>G [p.Met45Arg], c.207+1G>T) in arRP cases of Arab-Muslim, European, and Moroccan origin (Figure 1C). In this study, we identified two novel homozygous variants in *ARL2BP* in two unrelated RP cases that result in aberrant pre-mRNA splicing. Interestingly, the only missense variant identified is in exon 3 [10] (Figure 1C), suggesting a critical function of this exon in photoreceptor homeostasis.

One variant, c.207+1G>A, identified in this study occurs at the same location as a previously described mutation c.207+1G>T [11], and both variants cause exon 3 skipping (Figure 3). The other two splice site variants identified, c.101–1G>C [10] and c.390+5G>A, predominantly cause abnormal splicing, but evidence of low levels of wild-type *ARL2BP* transcript was detected in both cases (Figure 3) [10].

A comparison of the phenotypes described for all cases attributed to mutations in *ARL2BP* is presented in Table 1. In this study, the two probands presented at similar ages, although patient 2-III:2 (GC21134), in whom no normal transcript was detected, appeared to suffer more severe loss of the central retinal structure compared to patient 1-II:4. This may indicate the consequences of a decreased rather than a complete absence of ARL2BP protein, with residual levels of wild-type transcript and protein resulting in a milder phenotype. However, in the absence of animal models, further cases need to be described before any phenotype-genotype correlations can be made for this rare condition.

APPENDIX 1. INTERNATIONAL-STANDARD FULL-FIELD ERGS AND PATTERN ERG (PERG) FOR II:4, FAMILY 1.

To access the data, click or select the words "Appendix 1."

ACKNOWLEDGMENTS

We thank the patients for participating in this study and our funding bodies. This research was supported by grants from the National Institute for Health Research Biomedical Research Centre at Moorfields Eye Hospital National Health Service Foundation Trust, UCL Institute of Ophthalmology and Cambridge (UK), Fight For Sight (UK), Moorfields Eye Charity (UK), the Foundation Fighting Blindness (USA), Retinitis Pigmentosa Fighting Blindness (UK), National Institute for Health Research, NHS England, The Wellcome Trust, Cancer Research UK and The Medical Research Council. GA is supported by a Fight for Sight Early Career Investigator Award.

The UK Inherited Retinal Dystrophy Consortium includes Alison J. Hardcastle, Michel Michaelides, Vincent Plagnol, Nikolas Pontikos, Michael Cheetham, Gavin Arno, Alessia Fiorentino, Graeme Black, Georgina Hall, Rachel Gillespie, Simon Ramsden, Forbes Manson, Panagiotis Sergouniotis, Chris Inglehearn, Carmel Toomes, Manir Ali, Martin McKibbin, James Poulter, Emma Lord, Claire Smith, Kamron Khan, Andrea Nemeth, Susan Downes, Jing Yu, Stephanie Halford and Suzanne Broadgate.

REFERENCES

1. Ferrari S, Di Iorio E, Barbaro V, Ponzin D, Sorrentino FS, Parmeggiani F. Retinitis pigmentosa: genes and disease mechanisms. Curr Genomics 2011; 12:238-49. [PMID: 22131869].

2. Berson EL. Retinitis pigmentosa. The Friedenwald Lecture. Invest Ophthalmol Vis Sci 1993; 34:1659-76. [PMID: 8473105].

3. Nash BM, Wright DC, Grigg JR, Bennetts B, Jamieson RV. Retinal dystrophies, genomic applications in diagnosis and prospects for therapy. Transl Pediatr 2015; 4:139-63. [PMID: 26835369].

4. Rattner A, Sun H, Nathans J. Molecular genetics of human retinal disease. Annu Rev Genet 1999; 33:89-131. [PMID: 10690405].

5. Estrada-Cuzcano A, Roepman R, Cremers FP, den Hollander AI, Mans DA. Non-syndromic retinal ciliopathies: translating gene discovery into therapy. Hum Mol Genet 2012; 21:R1R111-24. [PMID: 22843501].

6. May-Simera H, Nagel-Wolfrum K, Wolfrum U. Cilia - The sensory antennae in the eye. Prog Retin Eye Res 2017; 60:144-180. [PMID: 28504201].

7. Reiter JF, Leroux MR. Genes and molecular pathways underpinning ciliopathies. Nat Rev Mol Cell Biol 2017; 18:533-547. [PMID: 28698599].

8. Pazour GJ, Rosenbaum JL. Intraflagellar transport and cilia-dependent diseases. Trends Cell Biol 2002; 12:551-5. [PMID: 12495842].

9. Roepman R, Wolfrum U. Protein networks and complexes in photoreceptor cilia. Subcell Biochem 2007; 43:209-35. [PMID: 17953396].

10. Davidson AE, Schwarz N, Zelinger L, Stern-Schneider G, Shoemark A, Spitzbarth B, Gross M, Laxer U, Sosna J, Sergouniotis PI, Waseem NH, Wilson R, Kahn RA, Plagnol V, Wolfrum U, Banin E, Hardcastle AJ, Cheetham ME, Sharon D, Webster AR. Mutations in ARL2BP, encoding ADP-ribosylation-factor-like 2 binding protein, cause autosomal-recessive retinitis pigmentosa. Am J Hum Genet 2013; 93:321-9. [PMID: 23849777].

11. Audo I, El Shamieh S, Mejecase C, Michiels C, Demontant V, Antonio A, Condroyer C, Boyard F, Letexier M, Saraiva JP, Blanchard S, Mohand-Said S, Sahel JA, Zeitz C. ARL2BP mutations account for 0.1% of autosomal recessive rod-cone dystrophies with the report of a novel splice variant. Clin Genet 2017; 92:109-11. [PMID: 27790702].

12. Carss KJ, Arno G, Erwood M, Stephens J, Sanchis-Juan A, Hull S, Megy K, Grozeva D, Dewhurst E, Malka S, Plagnol V, Penkett C, Stirrups K, Rizzo R, Wright G, Josifova D, Bitner-Glindzicz M, Scott RH, Clement E, Allen L, Armstrong R, Brady AF, Carmichael J, Chitre M, Henderson RH, Hurst J, MacLaren RE, Murphy E, Paterson J, Rosser E, Thompson DA, Wakeling E, Ouwehand WH, Michaelides M, Moore AT. Consortium NI-BRD, Webster AR, Raymond FL. Comprehensive Rare Variant Analysis via Whole-Genome Sequencing to Determine the Molecular Pathology of Inherited Retinal Disease. Am J Hum Genet 2017; 100:75-90. [PMID: 28041643].

13. Arno G, Agrawal SA, Eblimit A, Bellingham J, Xu M, Wang F, Chakarova C, Parfitt DA, Lane A, Burgoyne T, Hull S, Carss KJ, Fiorentino A, Hayes MJ, Munro PM, Nicols R, Pontikos N, Holder GE. Ukirdc, Asomugha C, Raymond FL, Moore AT, Plagnol V, Michaelides M, Hardcastle AJ, Li Y, Cukras C, Webster AR, Cheetham ME, Chen R. Mutations in REEP6 Cause Autosomal-Recessive Retinitis Pigmentosa. Am J Hum Genet 2016; 99:1305-15. [PMID: 27889058].

14. Lek M, Karczewski KJ, Minikel EV, Samocha KE, Banks E, Fennell T, O'Donnell-Luria AH, Ware JS, Hill AJ, Cummings BB, Tukiainen T, Birnbaum DP, Kosmicki JA, Duncan LE, Estrada K, Zhao F, Zou J, Pierce-Hoffman E, Berghout J, Cooper DN, Deflaux N, DePristo M, Do R, Flannick J, Fromer M, Gauthier L, Goldstein J, Gupta N, Howrigan D, Kiezun A, Kurki MI, Moonshine AL, Natarajan P, Orozco L, Peloso GM, Poplin R, Rivas MA, Ruano-Rubio V, Rose SA, Ruderfer DM, Shakir K, Stenson PD, Stevens C, Thomas BP, Tiao G, Tusie-Luna MT, Weisburd B, Won HH, Yu D, Altshuler DM, Ardissino D, Boehnke M, Danesh J, Donnelly S, Elosua R, Florez JC, Gabriel SB, Getz G, Glatt SJ, Hultman CM, Kathiresan S, Laakso M, McCarroll S, McCarthy MI, McGovern D, McPherson R, Neale BM, Palotie A, Purcell SM, Saleheen D, Scharf JM, Sklar P, Sullivan PF, Tuomilehto J, Tsuang MT, Watkins HC, Wilson JG, Daly MJ, MacArthur DG, Exome Aggregation C. Analysis of protein-coding genetic variation in 60,706 humans. Nature 2016; 536:285-91. [PMID: 27535533].

15. Raczy C, Petrovski R, Saunders CT, Chorny I, Kruglyak S, Margulies EH, Chuang HY, Kallberg M, Kumar SA, Liao A, Little KM, Stromberg MP, Tanner SW. Isaac: ultra-fast whole-genome secondary analysis on Illumina sequencing platforms. Bioinformatics 2013; 29:2041-3. [PMID: 23736529].

16. Pontikos N, Yu J, Blanco-Kelly F, Vulliamy T, Wong TL, Murphy C, Cipriani V, Fiorentino A, Arno G, Greene D, Jacobsen JO, Clark T, Gregory DS, Nemeth A, Halford S, Downes S, Black GC, Webster AR, Hardcastle A, Plagnol V. Phenopolis: an open platform for harmonization and analysis of sequencing and phenotype data. bioRxiv 2016; 33:2421-2423. .

17. Plagnol V, Curtis J, Epstein M, Mok KY, Stebbings E, Grigoriadou S, Wood NW, Hambleton S, Burns SO, Thrasher AJ, Kumararatne D, Doffinger R, Nejentsev S. A robust model for read count data in exome sequencing experiments and implications for copy number variant calling. Bioinformatics 2012; 28:2747-54. [PMID: 22942019].

18. Reese MG, Eeckman FH, Kulp D, Haussler D. Improved splice site detection in Genie. J Comput Biol 1997; 4:311-23. [PMID: 9278062].

19. Hebsgaard SM, Korning PG, Tolstrup N, Engelbrecht J, Rouze P, Brunak S. Splice site prediction in Arabidopsis thaliana pre-mRNA by combining local and global sequence information. Nucleic Acids Res 1996; 24:3439-52. [PMID: 8811101].

Articles are provided courtesy of Emory University and the Zhongshan Ophthalmic Center, Sun Yat-sen University, P.R. China. The print version of this article was created on 31 August 2018. This reflects all typographical corrections and errata to the article through that date. Details of any changes may be found in the online version of the article.